PHYSICAL REVIEW A **84**, 061404(R) (2011)

Time delay between photoemission from the 2*p* and 2*s* subshells of neon

L. R. Moore, M. A. Lysaght,* J. S. Parker, H. W. van der Hart,† and K. T. Taylor
Centre for Theoretical Atomic, Molecular and Optical Physics, Queen's University Belfast, Belfast BT7 1NN, United Kingdom
(Received 1 September 2011; published 15 December 2011)

The *R*-matrix incorporating time (RMT) method is a method developed recently for solving the time-dependent Schrödinger equation for multielectron atomic systems exposed to intense short-pulse laser light. We have employed the RMT method to investigate the time delay in the photoemission of an electron liberated from a 2*p* orbital in a neon atom with respect to one released from a 2*s* orbital following absorption of an attosecond xuv pulse. Time delays due to xuv pulses in the range 76–105 eV are presented. For an xuv pulse at the experimentally relevant energy of 105.2 eV, we calculate the time delay to be 10.2 ± 1.3 attoseconds (as), somewhat larger than estimated by other theoretical calculations, but still a factor of 2 smaller than experiment. We repeated the calculation for a photon energy of 89.8 eV with a larger basis set capable of modeling correlated-electron dynamics within the neon atom and the residual Ne^+ ion. A time delay of 14.5 ± 1.5 as was observed, compared to a 16.7 ± 1.5 as result using a single-configuration representation of the residual Ne^+ ion.

DOI: 10.1103/PhysRevA.84.061404 PACS number(s): 32.80.Aa, 32.80.Fb, 31.15.A−

One of the goals of attosecond science is to provide insights into the behavior of atomic electrons by imaging and controlling electronic motion using intense laser beams [1]. Recent advances in attosecond technology allow the delivery of light pulses with high intensity and with durations in the attosecond (as) range [2,3]. Such revolutionary laser technology is enabling time-resolved measurements of correlated-electron dynamics in atomic systems. One such tool for achieving time resolution on the sub-100-as time scale is attosecond streaking [4,5].

Attosecond streaking is based on a pump-probe experiment, in which an extreme ultraviolet (xuv) pulse of duration a few hundred attoseconds is used as the pump and a low-intensity phase-controlled few-cycle infrared (ir) pulse as the probe. The time delay between the two fields is varied but is such that the xuv and ir pulses overlap in time. The xuv pulse causes the emission of a photoelectron. Upon ejection, this electron is accelerated by the ir field. Its final energy and momentum depend on the value of the ir vector potential at the moment of its escape. Thus information on the time of ejection of the electron is embedded in its final escape energy.

Recently an attosecond streaking experiment investigated the time delay in photoemission of electrons liberated from the 2*p* orbitals of neon atoms with respect to those released from the 2*s* orbital by the same xuv light pulse [6]. This time delay was measured to be 21 ± 5 as, suggesting a small delay time between the formation of electron wave packets originating from the two different valence subshells. Theoretical calculations suggest that the delay is substantially smaller than the measured value. An independent electron model with a correlation correction calculated the delay to be 6.4 as [6]. An independent method using Hartree-Fock (HF) phase derivatives together with the random phase approximation with exchange (RPAE) correction for correlation calculated the delay to be 8.4 as [7].

The question arises as to whether the discrepancies between theory and experiment are related to the way in which the many-electron correlation effects are handled in the theoretical descriptions of the laser-atom interactions. Both theoretical methods mentioned above added a correlation correction *ad hoc*. It is possible that a solution of the full time-dependent Schrödinger equation (TDSE) taking multielectron correlation effects directly into account could modify the theoretical results.

We have recently developed an *ab initio* method for solving directly and accurately the TDSE describing the detailed response of multielectron atoms and ions to short, intense pulses of laser light: the *R*-matrix incorporating time (RMT) method [8,9]. The RMT method utilizes the powerful *R*-matrix theory *division-of-space* concept [10] to split the position space occupied by the atomic electrons into two regions: a multielectron inner region and an outer region in which one outer electron has become separated from the other electrons. In the multielectron inner region, electron-electron interactions are fully described and multielectron atom-laser Hamiltonian matrix elements are calculated explicitly. The multielectron wave function in this region is constructed from basis functions which have the form of a close-coupling expansion with pseudostates [10]. In the outer region only one electron is present and the electron there, besides experiencing the laser field directly, is aware of the remainder of the atomic system only via long-range multipole interactions. This effective one-electron problem is solved using state-of-the-art grid-based technology [11]. In both spatial regions the TDSE is integrated using high-order explicit time propagator methods [12]. A central concept of the RMT method, namely, the matching of a finite-difference representation in one region with a basis set representation in the other, was first developed using the hydrogen atom as a testing ground [13].

In this Rapid Communication, we present an application of RMT to the time delay between photoemission from the 2*s* and 2*p* subshells of a neon atom. Laser pulse parameters are chosen to closely resemble those used in the experiment [6]. The 800-nm ir field has an intensity of 10^{11} W/cm^2 and is linearly polarized in the z direction. It is a three-cycle pulse

*Present address: Department of Physics and Astronomy, The Open University, Walton Hall, Milton Keynes MK7 6AA, UK.
†h.vanderhart@qub.ac.uk

 ©2011 American Physical Society

with a $\sin^2$ profile. The xuv pulse has a central photon energy of 105.2 eV and peak intensity of 10^{13} W/cm^2. It is also linearly polarized in the z direction and has a Gaussian profile with a full width at half maximum (FWHM) in intensity of 270 as.

The RMT inner region has a radius of 20 a.u. The multielectron wave function in this region is expanded on a basis of field-free R-matrix eigenfunctions. The R-matrix basis used is one developed for single-photon ionization of Ne [14]. Our calculations include both the $1s^2 2s^2 2p^5\ ^2P^o$ ground state and the $1s^2 2s 2p^6\ ^2S^e$ excited state of Ne^+, so that emission of both a $2p$ electron and of a $2s$ electron is accounted for in the same calculation. In the present calculations both ionic states are represented by single configurations using HF orbitals for the $^2P^o$ ground state of the ion. The description of Ne includes all $1s^2 2s^2 2p^5 \epsilon l$ and all $1s^2 2s 2p^6 \epsilon l$ channels up to a given total angular momentum $L = L_{\max}$, where $L_{\max} = 9$. The ionization potential of the ground state is set to the experimental value [15]. The RMT outer region radial wave function is discretized on a finite difference grid extending to 6600 a.u. with a grid spacing of 0.2 a.u.

In the time integration we use a time step of 0.0125 a.u. Typically we let the calculation run for a further 15 000 time steps after the ir laser pulse has passed. This allows the ejected electronic wave packets to propagate to regions far from the nucleus where the Coulombic field of the residual ion is weak. We have checked all parameter settings (including the radius of the inner region) used in the code to ensure that the results are converged. Similarly we have checked the laser parameters to ensure they have no effect on the results. The only exception we have found is that reducing the duration of the xuv pulse can have an impact on the time delay: At extremely short durations the Fourier transform of the pulse profile itself can have substantial side wings, effectively introducing additional xuv frequencies into the calculation.

Upon completion of the time propagation, the outer-electron wave function needs to be decoupled from the full multielectron wave function [16]. This outer-electron wave function is then transformed to momentum space under the assumption that the long-range Coulomb potential is negligible, a valid assumption since the ejected electronic wave packets are propagated to regions sufficiently far from the nucleus so that a field-free spherical wave transformation is satisfactory.

Figure 1 displays momentum spectra in the x-z plane of the outgoing electron for the two cases of the xuv field delayed, relative to the ir field, by (a) $1.25T_{\rm ir}$ and (b) $1.75T_{\rm ir}$, where $T_{\rm ir}$ is the ir laser field period. In Fig. 1(a) the peak intensity of the xuv field coincides with a minimum in the ir vector potential and in Fig. 1(b) with a maximum. Because the drift momentum P_z of the outgoing electron is equal to the charge on the electron (-1) times the value of the ir vector potential at the time of emission, the momentum spectrum is shifted upward in Fig. 1(a) and downward in Fig. 1(b) relative to a position centered on the origin. Visible in both plots of Fig. 1 are two rings. The outer (inner) ring represents the component of the outgoing wave packet arising from ionization of the $2p$ ($2s$) subshell.

Further calculations are carried out at different delays between the xuv and ir fields. For each delay, the shifts of both the inner and the outer rings of the momentum spectrum are calculated. These shifts correspond to the additional momentum P_z, imparted by the ir field, gained by electrons emitted from the $2s$ and from the $2p$ subshells, respectively. Figure 2(a) plots these shifts as a function of delay between the xuv and ir fields. As is evident from Fig. 2(b), the shifts of the momentum distributions are not identical for electrons emitted from the two different valence shells: They exhibit a small temporal shift with respect to one another. It is as though the electrons emitted from the two valence shells experience a slightly different ir vector potential at the moment of release, thus suggesting a time delay in photoemission as observed experimentally. By fitting a polynomial through the data points shown in Fig. 2(b), we calculate that an electron emitted from the $2p$ orbital is delayed by 10.2 as, relative to one released from the $2s$ orbital. The use of fitting procedures also provides a measure of the accuracy with which the delay can be extracted from our calculations. Furthermore, we have repeated the calculations using a variety of xuv pulse profiles. Through these additional investigations, we estimate the standard deviation in our calculated time delay to be 1.3 as.

Table I presents a comparison of our calculated value for the time delay with other values calculated both numerically and experimentally. The RMT result is slightly higher than the other theoretical results, but it too lies substantially below the experimental result.

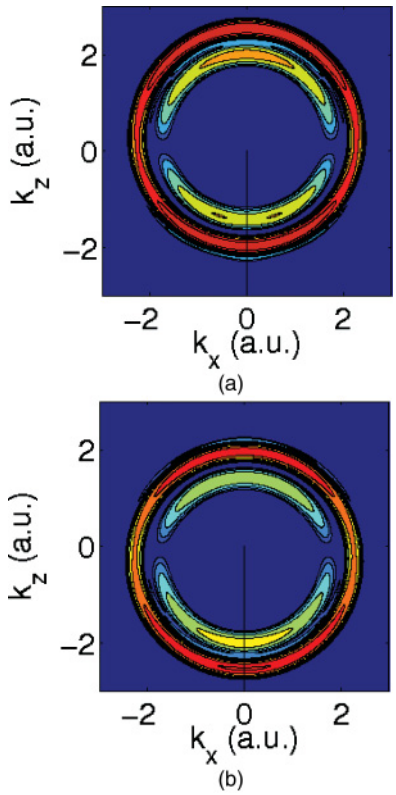

FIG. 1. (Color online) Momentum spectra in the x-z plane obtained for the two cases of the xuv field delayed, relative to the ir field, by (a) $1.25T_{\rm ir}$ and (b) $1.75T_{\rm ir}$. In this example the intensity of the ir field is increased to 10^{13} W/cm^2.

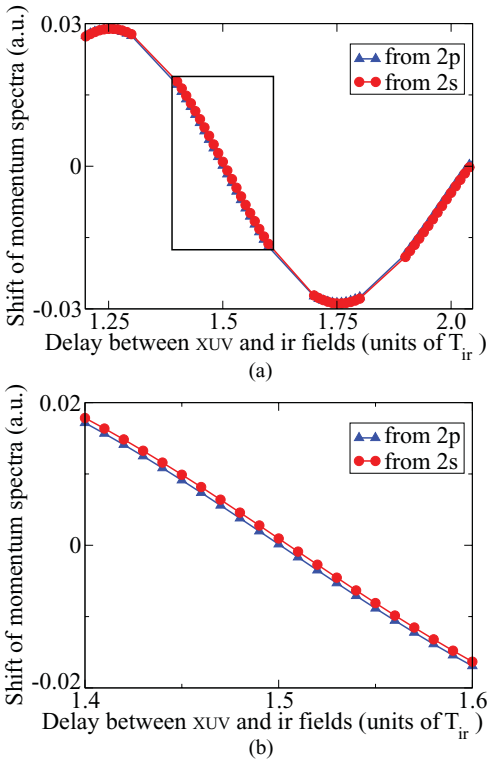

FIG. 2. (Color online) The shifts of the momentum distributions of electrons ejected from the $2s$ and from the $2p$ subshells as a function of the delay between the xuv and ir fields. (b) Magnification of the region enclosed by the black box in (a).

To establish the dependence of the time-delay difference on photon energy, we have repeated the calculations at several xuv photon energies. Figure 3 shows that as the xuv photon energy is decreased from 105.2 to 77.4 eV, the time delay in photoemission increases from 10.2 to 26.7 as.

One of the strengths of RMT is its ability to describe multielectron excitations that may occur within the parent atom and the residual ion. We have repeated the time-delay calculation using a greatly enlarged basis set for Ne^+. This basis is capable of including all single and double excitations from $2s2p^6$ and $2s^22p^5$ to a set of pseudo-orbitals $\overline{3s}$, $\overline{3p}$, and $\overline{3d}$. As a consequence, for Ne, all single, double, and triple excitations from $2s^22p^6$ to $\overline{3s}$, $\overline{3p}$, and $\overline{3d}$ are included. Details of these orbital functions can be found in

TABLE I. Comparison of time delays between photoemission from the $2p$ and $2s$ subshells of neon following absorption of an attosecond xuv pulse of photon energy 105–106 eV.

Group	Method	Delay (as)
Schultze *et al.* [6]	Experiment	21 ± 5
Schultze *et al.* [6]	Independent electron model	4.0
	Correlation correction	2.4
	Total	6.4
Kheifets *et al.* [7]	HF phase derivatives	6.2
	RPAE correction	2.2
	Total	8.4
Present work	RMT	10.2 ± 1.3

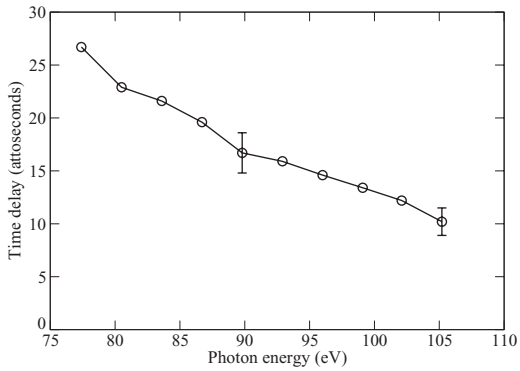

FIG. 3. Time delay in photoemission as a function of xuv photon energy. The error bars shown on two of the data points are ± one standard deviation. The time delays were calculated using a single-configuration representation of the wave function.

Ref. [14]. The calculation uses an xuv photon energy of 89.8 eV (for reasons described below). At this energy the average value of the time delay is found to be 14.5 as with a standard deviation of 1.5 as. This compares to a value of 16.7 as obtained using the single-configuration representation. The single-configuration results are shown in Fig. 3. The error bar gives the estimated standard deviation (1.9 as) at 89.8 eV.

We cannot at present perform the larger basis set calculation on the full range of frequencies in Fig. 3. Attempts to do this at 105.2 eV, for example, failed because strong pseudoresonances were encountered [14]. These pseudoresonances represent channels omitted from the configuration-interaction representation of the wave function, and their effect is to introduce an additional, potentially spurious, structure into the momentum spectrum of the outgoing wave packet. The resulting uncertainty in the time-delay measurement overwhelms the measurement itself.

The data points obtained at 89.8 eV nevertheless provides us with a preliminary estimate of uncertainties in the calculations that arise from various truncations of the R-matrix basis sets. We cannot claim that the observed decrease in time delay is significant, but it points to the possibility that the time delay in photoemission is sensitive to atomic structure and to the various excitations that may be possible within that structure, and suggests that future exploration of this possibility is warranted.

Finally, we review some of the difficulties that will inevitably be encountered in the future as attempts are made to improve on the present analysis of this problem. Exploration of atomic-structure effects, especially at 105.2 eV, is complicated by the large number of double continua and double Rydberg states that are available. These include not only double continua attached to the $2s^22p^4$ and $2s2p^5$ thresholds of Ne^{2+}, but also double continua and Rydberg series attached to the $2s^22p^33s$, $2s^22p^33p$ and $2s^22p^33d$ thresholds of Ne^{2+}. For example, $2s^22p^33d^24s$ states could be excited by single-photon absorption from the $2s^22p^6$ ground state via an admixture of $2s^22p^43d^2$. Such excitations can be interpreted as the excitation of one $2p$ electron with a simultaneous collective excitation of the residual five $2p$ electrons. An

accurate description of the resonance structure thus requires a detailed description of triple excitations. The number of Ne^+ states that need to be included as target states to describe $2s^2 2p^3 3d^2 4s$ resonances exceeds 150, even if only excitations to $3s$, $3p$, and $3d$ are included. A time-dependent calculation with this number of target states is not feasible at present using our numerical methods, even on the largest available massively parallel computers. The inclusion of double continua is also nontrivial, and, to the best of our knowledge, no group has attempted such calculations for the full Ne atom. Experiments at a lower photon energy, ∼75 eV, would therefore be very useful, as this will greatly reduce the complexity of theoretical calculations.

In summary, we have applied the RMT method to the investigation of the time delay in photoemission from the $2s$ and $2p$ subshells of neon following absorption of an attosecond xuv pulse. In order to reduce systematic differences between experiment and theory, we have used a similar approach as an experiment in the analysis of our results. At an xuv photon energy of 105.2 eV, we calculate a value for the time delay of 10.2 ± 1.3 as. To date, all theoretical calculations of this time delay fall short of the experimental measurement of 21 ± 5 as. The RMT method yields a value for the time delay that is somewhat larger than the other theoretical calculations and that lies within two to three standard deviations of the experimental measurement.

We find that extraction of the time delay is extremely sensitive to even small features in the momentum spectra which can have an impact on the fitting processes. However, analysis of the experimental data must also be subject to these issues. To extract a value for the time delay, the experimental data are analyzed using a frequency-resolved optical gating (FROG) phase-retrieval algorithm [17] which has been specially tailored for attosecond measurements. It does interpolate the spectrogram along the energy axis, but avoids interpolating along the delay axis. To enable a better comparison with experiment, it may be interesting for future theoretical work to generate full spectrograms which could then be subsequently analyzed using the same FROG phase-retrieval algorithm.

L.R.M., H.W.v.d.H., and K.T.T. acknowledge funding from the UK Engineering and Physical Sciences Research Council. M.A.L. and J.S.P. acknowledge funding under the HECToR distributed CSE program, which is provided through The Numerical Algorithms Group (NAG), Ltd.

[1] P. B. Corkum and F. Krausz, Nat. Phys. **3**, 381 (2007).
[2] M. F. Kling *et al.*, New. J. Phys. **10**, 025024 (2008).
[3] G. Sansone *et al.*, Science **314**, 443 (2006).
[4] E. Goulielmakis *et al.*, Science **305**, 1267 (2004).
[5] R. Kienberger *et al.*, Nature (London) **427**, 817 (2004).
[6] M. Schultze *et al.*, Science **328**, 1658 (2010).
[7] A. S. Kheifets and I. A. Ivanov, Phys. Rev. Lett. **105**, 233002 (2010).
[8] L. R. Moore, M. A. Lysaght, L. A. A. Nikolopoulos, J. S. Parker, H. W. van der Hart, and K. T. Taylor, J. Mod. Opt. **58**, 1132 (2011).
[9] M. A. Lysaght, L. R. Moore, L. A. A. Nikolopoulos, J. S. Parker, H. W. van der Hart, and K. T. Taylor, in *Quantum Dynamic Imaging: Theoretical and Numerical Methods*, edited by A. D. Bandrauk and M. Ivanov (Springer, Berlin, 2011), pp. 107–134.
[10] P. G. Burke and K. A. Berrington, *Atomic and Molecular Processes: An R-matrix Approach* (IOP, Bristol, 1993).
[11] E. S. Smyth, J. S. Parker, and K. T. Taylor, Comput. Phys. Commun. **114**, 1 (1998).
[12] W. E. Arnoldi, Q. Appl. Math. **9**, 17 (1951).
[13] L. A. A. Nikolopoulos, J. S. Parker, and K. T. Taylor, Phys. Rev. A **78**, 063420 (2008).
[14] P. G. Burke and K. T. Taylor, J. Phys. B **8**, 2620 (1975).
[15] E. B. Saloman and C. J. Sansonetti, J. Phys. Chem. Ref. Data **33**, 1113 (2004).
[16] H. W. van der Hart, M. A. Lysaght, and P. G. Burke, Phys. Rev. A **77**, 065401 (2008).
[17] J. Gagnon, E. Goulielmakis, and V. S. Yakovlev, Appl. Phys. B **92**, 25 (2008).